Phase stability and hydrogen desorption in a quinary equimolar mixture of light-metals borohydrides

Phase stability and hydrogen desorption in a quinary equimolar mixture of light-metals borohydrides

Erika Michela Dematteis,[a)b)] Antonio Santoru,[b)] Marco Gabriele Poletti,[a)] Claudio Pistidda,[b)] Thomas Klassen,[b)] Martin Dornheim[b)] and Marcello Baricco[a)*]

[a)]Department of Chemistry and NIS-CrisDi-INSTM, University of Turin, Via Pietro Giuria 7, 10125 Torino, Italy

[b)]Nanotechnology Department, Helmholtz-Zentrum Geesthacht Max-Planck Straße 1, 21502, Geesthacht, Germany

*Corresponding author

Marcello Baricco

E-mail address: marcello.baricco@unito.it

Tel.: +39 011 6707569

Fax: +39 0116707856

Abstract

The present study aims at investigating, for the first time, a quinary mixture of light-metals borohydrides. The goal is to design combinations of borohydrides with multiple cations in equimolar ratio, following the concept of high entropy alloys. The equimolar composition of the $LiBH_4$-$NaBH_4$-KBH_4-$Mg(BH_4)_2$-$Ca(BH_4)_2$ system was synthetized by ball milling. The obtained phases were analysed by X-ray diffraction and *in-situ* Synchrotron Radiation Powder X-ray Diffraction, in order to establish the amount of cations incorporated in the obtained crystalline phases and to study the thermal behaviour of the mixture. HP-DSC and DTA were also used to define the phase transformations and thermal decomposition reactions, leading to the release of hydrogen, that was detected by MS. The existence of a quinary liquid borohydride phase is reported for the first time. Effects of the presence of multi-cations compounds or a liquid phase on the hydrogen desorption reactions are described.

Keywords: complex hydrides, borohydride, entropy, hydrogen storage.

Introduction

In the last decades, research focused on the synthesis and characterization of new borohydrides.[1,2] Anion substitution in borohydrides has been demonstrated to provide solid solutions[3–11], as well as hydrogen-fluorine exchange.[12–15] On the other hand, by mixing different light-metals borohydrides, the formation of bimetallic and trimetallic compounds or solid solutions were evidenced, often forming eutectic mixtures. New applications of bimetallic compounds have been suggested.[1] In few cases, borohydrides or their eutectic mixtures have been nanostructured with carbon materials, or nanoconfined, or mixed to form reactive hydride composites, showing improved hydrogen release and cyclability.[16–19] For some binary and ternary mixtures of borohydrides, corresponding thermodynamic properties and phase diagrams have been recently assessed.[20,21]

For the present work, the approach is to design combinations of borohydrides with multiple cations in equimolar ratio, following the concept of high entropy alloys.[22,23] In High Entropy Alloys (HEAs) at least 5 elements should be present in concentrations between 5 and 35 atomic percent, so that the high entropy of mixing can stabilise the formation of solid solutions with simple crystal structures. However, if the formation enthalpy of an intermetallic compound is high enough to overcome the effect of entropy, that intermetallic compound will be present in the equilibrium mixture.

HEAs and relative concepts were born within the metallurgy community. In 2004 Cantor[22] and Yeh[24] suggested to discover new properties and alloys exploring the central region of the phase space in systems with at least five components. This leaded to the findings of microstructures mainly composed of *fcc* or *bcc* multicomponent solid solutions.[25,26] Since 2004, many HEAs have been explored, finding in some cases very interesting properties for compositions containing high entropy phases. In particular, mechanical behaviour of HEAs has been investigated.[27,28] An

operative way to define a high entropy phase is to start from the calculation of the configurational entropy, ΔS_{conf}, of a completely disordered solid solution with the Boltzman formula,

$$\Delta S_{conf} = -R \cdot \Sigma^{i} x_i \cdot \ln(x_i) \quad (1)$$

being x_i the atomic fraction of the *i-th* elements. Commonly, the disordered solid solutions with $\Delta S_{conf} > 1.5$ R, where R is the gas constant, are defined high entropy phases.[29] Complex Concentrated Alloys (CCAs) are alloys showing a nominal composition with a configurational entropy of a hypothetical completely random state, i.e. $\Delta S_{conf} > 1.5$ R, but composed of more complex microstructures, i.e. constituted by different phases and intermetallics, but representative of the inner part of multicomponent phase space.[30]

In the case of equimolar compositions, the value of ΔS_{conf} can be obtained, for a system with a defined number of components N, as:

$$\Delta S_{conf} = R \cdot \ln(N) \quad (2)$$

The higher the number of components N, the higher the value reachable by ΔS_{conf} in the system, i.e. for N = 5, $\Delta S^{max}_{conf} = 1.61$ R, for N = 6, $\Delta S^{max}_{conf} = 1.79$ R and for N= 7, $\Delta S^{max}_{conf} = 1.95$ R.

Ordering in high entropy phases have been experimentally found in the exploration of CCAs.[31–33] Ordering decreases the entropy of the phase, since, following the Compound Energy Formalism (CEF),[34] the configurational entropy ΔS_{conf} should be decomposed into the contributes of the respective sub-lattices. Considering, for example, a system containing two different sub-lattice *h*, with a number of sites X, and *k,* with a number of sites Y, the configurational entropy of the ordered structure can be defined as:

$$\Delta S^{ORD}_{conf} = -R \cdot (X/(X+Y) \cdot \Sigma^{i} y^{h}_{i} \ln(y^{h}_{i}) + Y/(X+Y) \cdot \Sigma^{i} y^{k}_{i} \ln(y^{k}_{i})) \quad (3)$$

where y^{h}_{i} and y^{k}_{i} are the mole fractions of the constituent *i* in the sublattice *h* and *k*, respectively.[31] For instance, in a AB compound with atoms A and B in two different sub-lattices *h* and *k* with X and Y equal to 1, the respective disordering of each sublattices (considering random mixing within each sub-lattice) obtained replacing half atoms of A with C in sub-lattice *h* and half

atoms of B with D in sub-lattice *k*, leading to an (ACBD) solid solution, increases the configurational entropy of 0.69 R, a value comparable to the configurational entropy of a equimolar binary system completely disordered. Such a situation can be observed in ionic compounds, which are characterized mainly by two sub-lattices, a cationic and an anionic one.

Recently, the formation of entropy stabilized mixtures of oxides[35] and borides[36] was reported, together with the description of a entropy driven polymorphic transition as a function of the composition of the solid solution. In ionic compounds, a structure containing one sub-lattice with random cation occupancy can be obtained at a sufficient high temperature if it does not melt before such a transition. In the case of oxides, electroneutrality and geometrical parameters must be taken into account to succeed in the formation of a solid solution. Generally, cations chosen for the equimolar mixture should come from compounds with the same crystal structures, should have similar ionic radii and coordination number. In addition, they should be isovalent among them and with the counter anion. The formation of a multi cation solid solution can be correlated with the Goldschmidt tolerance factor (t), which should be close to 1.[37] The cation-size difference (δ_R) or average size difference using the lattice constant of individual component (δ_a and δ_c) should also be considered as important factor for the formation of one-phase solid solution if the compounds have mixed ionic and covalent characteristics. In the case of borides, δ_a and δ_c should be in the range of 4-12%. In addition, enthalpy of mixing, entropy of mixing and melting temperature play a role as for HEAs, but they usually are thermodynamic parameters unknown for all phases and of difficult experimental determination.

Unlike alloys, oxides and diborides, the most common and studied borohydrides presents different crystal structures, polymorphs, and many bi- or trimetallic compounds are present in binary or higher mixtures, as reported in **Table 1**.

Table 1 – Borohydrides structures and details on bimetallics, solid solutions (SS), enthalpy and temperature of polymorphic transition (PT), eutectic melting or thermal minima (EU/TM), decomposition (DEC).

	$LiBH_4$	$NaBH_4$	KBH_4	$Mg(BH_4)_2$	$Ca(BH_4)_2$
$LiBH_4$	Orthorhombic (*Pnma*) Hexagonal ($P6_3mc$) $T_{PT\ ORT-HEX}$ = 115 °C ΔH_{PT} = 5.3 kJ/mol T_M = 280 °C ΔH_M = 7.2 kJ/mol[38] T_{DEC}>400 °C[39]	0.70$LiBH_4$-0.30$NaBH_4$ $T_{PT\ ORT-HEX}$ = 95 °C T_{EU} = 216 °C ΔH_M = 7.0 kJ/mol[20] T_{DEC}>400 °C[40] SS cubic, orthorhombic, hexagonal[20]	0.725$LiBH_4$-0.275KBH_4 T_{EU} = 104 °C ΔH_M = 11.0 kJ/mol[41] T_{DEC}>400 °C[42] $LiK(BH_4)_2$: Orthorhombic (Pnma)[41]	0.55$LiBH_4$-0.45$Mg(BH_4)_2$ T_{EU} = 180 °C[43] T_{DEC}>250 °C[43–45]	0.68$LiBH_4$-0.32$Ca(BH_4)_2$ T_{EU} = 200 °C[46] ΔH_M = 9.1 kJ/mol[47] T_{DEC}>350 °C[46]
$NaBH_4$		Cubic ($Fm\bar{3}m$) T_M = 505 °C ΔH_M = 16.9 kJ/mol[48] T_{DEC}>505 °C[48]	0.682$NaBH_4$-0.328KBH_4 T_{TM} = 462 °C ΔH_{TM} = 17.0 kJ/mol[49] SS cubic[49] T_{DEC}>465 °C[49]	0.40$NaBH_4$-0.60$Mg(BH_4)_2$ T_{EU} = 205 °C ΔH_M = 7.0 kJ/mol[50] T_{DEC}>205 °C[50]	Partial Melting[50] T_{DEC}>350 °C[50]
KBH_4			Cubic ($Fm\bar{3}m$) T_M = 605 °C ΔH_M = 19.2 kJ/mol[21] T_{DEC}>605 °C[51]	$K_2Mg(BH_4)_4$: Monoclinic ($P2_1/n$)[52] $K_3Mg(BH_4)_5$: Tetragonal ($P4_2/mbc$)[52]	$KCa(BH_4)_3$: Orthorhombic ($Pba2$)[53]
$Mg(BH_4)_2$				α : Hexagonal ($P6_122$) β : Orthorhombic (*Fddd*) γ : Cubic ($Ia\bar{3}d$) metast. $T_{PT\ \alpha-\beta}$ = 184 °C[54] ΔH_{PT} = 11.3 kJ/mol[54] T_{DEC}>290 °C[51]	
$Ca(BH_4)_2$					α: Orthorhombic ($F2dd$) β: Tetragonal ($P\bar{4}$) $T_{PT\ \alpha-\beta}$ = 162 °C[55] ΔH_{PT} = 8.6 kJ/mol[55] T_{DEC}>300 °C[56]

Their crystal structures are characterized by the presence of cations surrounded by the complex BH_4^- anion. The presence of multiple cations is expected to promote the formation of solid solutions as observed for oxide systems or multi-cations eutectics. On the other hand, when the formation enthalpy of a multi-metallic compounds is high enough to overcome the entropy contribution to the free energy of solid solutions, their formation will be hindered.

The present study aims at extending the study on multi-metallic compounds and to explore, for the first time, a quinary mixture of borohydrides in the $LiBH_4$-$NaBH_4$-KBH_4-$Mg(BH_4)_2$-$Ca(BH_4)_2$ system. In fact, this approach appears to be promising from the hydrogen release point of view, owing to the presence of cations of light-metals borohydrides, showing low decomposition temperatures. The obtained phases were studied by Powder X-ray Diffraction (PXD) and *in-situ* Synchrotron Radiation Powder X-ray Diffraction (SR-PXD), in order to define the cell parameters and volumes of the phases, also as a function of temperature. The thermal behaviour of the mixtures were analysed by high-pressure differential scanning calorimetry (HP-DSC) and differential thermal analysis (DTA). This data were compared with the SR-PXD analysis to identify the phase transitions and reactions, while hydrogen release was studied by mass spectrometry (MS) and decomposition products were defined by PXD, attenuated total reflection infrared (ATR-IR) and Raman spectroscopies. The occurrence of solid solutions, multi cation eutectics and multi-metallic compounds leads to differences in the hydrogen desorption reactions, depending on the interaction among the components.

Experimental

Sample preparation

Lithium borohydride ($LiBH_4$, purity >95% from Sigma-Aldrich), sodium borohydride ($NaBH_4$, purity >98% from ABCR), potassium borohydride (KBH_4, purity >97% from Merck), magnesium borohydride (γ-$Mg(BH_4)_2$, purity >95% from Sigma Aldrich) and calcium borohydride (αβ-$Ca(BH_4)_2$, purity >99% from KatChem) were mixed by ball milling (BM) in equimolar ratio. A Fritsch Pulverisette 6 planetary mill was used to ball mill the reactants under 10 bar of H_2 in 250

mL stainless steel vials, with stainless steel balls (o.d. 10 mm) and a balls-to-sample mass ratio of 30:1. The pure borohydrides were milled for 1 h at 350 r.p.m., while the quinary mixture was milled at the same r.p.m. up to 50 hours.

A thermal treatment up to 500 °C was performed in an alumina crucible to check the phase stability. A quartz tube was used to hold the crucible and evacuate the inert gas; after evacuation, the tube was placed in a hoven, heated at the desired temperature and cooled down at 5 °C/min.

All preparations and manipulations of the samples were performed in argon-filled or nitrogen-filled glove boxes with a circulation purifier, with O_2 and H_2O levels lower than 1 ppm.

Characterization

Laboratory powder X-ray diffraction (PXD)

Powder X-ray diffraction measurements were performed at room temperature (*ex situ*) using a Panalytical X-pert (Cu K_α = 1.54059 Å, K_β = 1.54446 Å) in capillary transmission set-up (Debye-Scherer geometry). Patterns were collected from 5° to 130° 2θ range, step size 0.016, time step 90 seconds. Samples were inserted in 0.5 mm glass capillaries in the glove box and sealed with plastiline, then moved out of the glove box and sealed with flame.

The Rietveld refinement of diffraction patterns has been performed using the MAUD (Materials Analysis Using Diffraction) program.[57] The instrumental function was determined using pure Si as a standard.

In-situ time-resolved synchrotron radiation powder X-ray diffraction (SR-PXD)

The *in situ* SR-PXD measurement was performed at the diffraction beamline P02, in the Petra III storage ring of DESY (Hamburg, Germany). Few milligrams of sample were packed in a single crystal sapphire capillary (inner diameter ca. 0.6 mm). The capillary was then mounted in an in-house-built synchrotron cell and sealed using Vespel ferules and Swagelok connections. This cell is equipped with a heating element (electric resistance) and thermocouples allowing varying the temperature between RT and 450 °C during the experiment. Moreover, the cell can be connected to an external gas line and loaded with inert or reactive gases at different pressures.[58] The sample

was heated up to 250 °C and cooled down to room temperature (RT) at 5 °C/min under a hydrogen pressure of 1 bar. The beamline provides a monochromatic X-ray beam (λ = 0.207157 Å) and is equipped with a PerkinElmer XRD 1621 plate detector (pixel size 200 µm x 200 µm, array 2048x2048 pixels). The diffraction images, collected every 15 seconds, were integrated with the software Fit2D. The Rietveld refinement of selected diffraction patterns has been performed using the MAUD program.[57] The instrumental function was determined using LaB_6 as a standard.

High Pressure Differential scanning calorimetry (HP-DSC)

A high-pressure 204 Netzsch DSC was used to analyse the thermal behaviour of the mixture, avoiding decomposition and obtaining accurate value of temperature and enthalpy of phase transformations. Approximately 3 to 9 mg of sample were loaded into alumina or aluminium crucibles with lid. The DSC instrument is placed inside the glove box to ensure sample handling under inert atmosphere. Samples were heated and cooled in the desired temperature range at 5 °C/min under 1 or 50 bar of H_2.

Differential Temperature Analysis coupled with Mass Spectroscopy (DTA-MS)

A DTA Netzsch STA 409 coupled with a Hiden Analytical Hal 201 Mass Spectrometer was used to analyse hydrogen and diborane release in the mixture as a function of temperature. The instrument is placed inside the glove box to ensure sample handling under inert atmosphere. Approx. 2 mg of sample were heated from RT up to 500 °C at 5 °C/min under an argon gas flow of 50 mL/min, which was used also to transport the gases to the MS analyser.

Raman Spectroscopy

Raman spectra were collected using a WITec alpha300 confocal Raman spectrometer (Ulm, Germany) using a 633 nm (red) excitation wavelength in backscattering mode, with exposure times of 0.5 s and 200 accumulations per spectrum over a 2600–1000 cm^{-1} range.

Attenuated Total Reflectance Infrared Spectroscopy (ATR-IR)

The Infrared spectra (2 cm^{-1} resolution, average on 64 scans) were collected in Attenuated Total Reflection mode on loose powder with a Bruker Alpha-P spectrometer, equipped with a diamond

crystal. All the spectra were recorded in the 5000−400 cm^{-1} range, in a protected atmosphere since the instrument is placed inside a nitrogen filled glove-box (MBraun Lab Star Glove Box supplied with pure 5.5 grade Nitrogen, <1 ppm O_2, <1 ppm H_2O).

Results and Discussion

Equilibrium phases in the quinary borohydride system

After 50 hours of ball milling, the equimolar mixture of $LiBH_4$-$NaBH_4$-KBH_4-$Mg(BH_4)_2$-$Ca(BH_4)_2$ (LiNaKMgCa system) still presents all the pristine compounds ($LiBH_4$, $NaBH_4$, KBH_4, α-$Mg(BH_4)_2$ and α-$Ca(BH_4)_2$) plus $KCa(BH_4)_3$, as can be observed in the PXD pattern shown in **Figure 1A, BM**. It is worth noting that, in the mixture, $Mg(BH_4)_2$ and $Ca(BH_4)_2$ are present only in the α polymorph, but γ-$Mg(BH_4)_2$ and β-$Ca(BH_4)_2$ are not detected, even if they are present in the starting materials. Similar behaviour was observed in the $LiBH_4$-$Mg(BH_4)_2$ system, where the α-β transition of $Mg(BH_4)_2$ is reversible.[43] No other bi- or tri-metallic compounds have been observed to form under ball milling. The Rietveld refinement and cell parameters of ball milled pure borohydrides are reported in **Figure S1** and they can be compared with the cell parameters obtained from the Rietveld refinement of the LiNaKMgCa BM sample, reported in **Figure S2A**. In the case of starting BM γ-$Mg(BH_4)_2$ (**Figure S1D**), the PXD peaks are very weak because of the milling treatment, suggesting a significant reduction of long-range order in the structure upon mechano-chemical treatment. This result can be related to the amorphous phase of $Mg(BH_4)_2$ observed under pressure.[59] Since the $KCa(BH_4)_3$ is the only bimetallic compound that has been observed, an equimolar mixture of KBH_4 and $Ca(BH_4)_2$ (KCa system) was synthetized and investigated. The weight fraction and cell parameters of the ball milled KCa system are reported in **Figure S3A**. In the KCa system, after milling, an excess of KBH_4 and $Ca(BH_4)_2$ is present, together with the $KCa(BH_4)_3$ compound, suggesting an incomplete reaction after ball milling at the present conditions. After thermal cycling up to 370 °C, i.e. over the melting temperature of the bimetallic compound (**Figure S3B**), an excess of KBH_4 is still observed, as it was observed in the literature,[53] which suggests an off-stoichiometry of the compound. Generally, no marked changes

in the cell parameters of all phases are observed comparing the values observed for pure compounds and the LiNaKMgCa system, evidencing no significant solid solutions formation upon milling. The only sensible variation that can be noticed is related to a decrease of the *a* lattice parameter of $KCa(BH_4)_3$ in the quinary system (8.001 Å), with respect to that observed in the KCa system after annealing (8.018 Å). The lower value of this cell parameter in the quinary mixture might be related to the dissolution, inside the crystal structure of the bimetallic compound, of a low amount of cations (e.g. Li^+, Na^+ and Mg^{2+}) with a smaller size with respect to K^+ and Ca^{2+}.

Ball milled pristine borohydrides have been also compared with the KCa and LiNaKMgCa systems by means of ATR-IR and Raman spectroscopies and results are reported in **Figure 2A and Figure 2B, respectively**.

In ATR-IR spectra, bands in the 2400-2000 cm^{-1} region are related to the B-H stretching, while those in the 1300-800 cm^{-1} region are related to H-B-H bending vibrational modes of ionic BH_4^-.[1,11,60] The stretching (ν_1, ν_3) and bending (ν_2, ν_4) modes of the BH_4^- anions are reported in **Figure 2A** as dashed lines for comparison. The isolated BH_4^- anion has an ideal tetrahedral symmetry, but the vibrational modes can be split into several components in the crystalline state, due to lowering of its site symmetry. Generally, modes ν_3 and ν_4 are triply degenerate in free tetrahedral BH_4^- ions, and the ν_2 is doubly degenerate.[11] The single broad band that can be observed in **Figure 2A, BM** for the quinary mixture in the 2400-2000 cm^{-1} region may be related to a symmetry change of the BH_4^- site. However, since several phases are present simultaneously in the sample, there may be interaction among them, leading to disordering effects. So, the broad band extending in a wide energy region can be assigned to vibrational modes of BH_4^- ion in different borohydrides. Taking into account the results from PXD, broad bands observed in ATR-IR spectra are assigned to a physical mixture of different phases, rather than the presence of solid solutions.

Raman spectra confirm the presence of a single broad stretching band, in a frequency range similar to the ones of $LiBH_4$ and $Ca(BH_4)_2$, as it can be observed from dashed lines in **Figure 2B, BM**.

In conclusion, a unique solid solution has not been obtained upon mixing five different borohydrides by mechanical milling. Only the $KCa(BH_4)_3$ bimetallic compound has been formed, suggesting that it has a strong negative enthalpy of formation, that overcomes possible entropy of mixing contributions to the free energy of the mixture.

Thermal stability of the quinary borohydride system

The DSC traces, obtained upon heating the LiNaKMgCa system up to 200 °C and then cooling down to 60 °C, are reported in **Figure 1B**. Two cycles have been carried out and they evidence various events: the polymorphic transition of $KCa(BH_4)_3$ at T_{peak}= 76 °C (61 °C on cooling) and the melting of a eutectic at T_{peak}= 99 °C (90 °C on cooling). Another melting peak is observed at T_{peak}= 113 °C (95 °C on cooling), followed by another melting event ending at T= 130 °C. The liquidus temperature is observed at 180 °C (172 °C on cooling). On the first cooling ramp, only one peak is observed, possibly for segregation or kinetic reasons.

The PXD pattern of the quinary mixture after the DSC cycling up to 200 °C is shown in **Figure 1A, 200 °C**, and corresponding Rietveld refinement analysis is reported in **Figure S2B**. The PXD peaks of $KCa(BH_4)_3$ are rather intense and those of $NaBH_4$ are clearly observed, while only traces of $LiBH_4$, KBH_4, α-$Mg(BH_4)_2$ and α-$Ca(BH_4)_2$ are still visible, together with a broad halo.

After thermal cycling the LiNaKMgCa system up to 200 °C, the ATR-IR bands in the 1300-800 cm^{-1} region became more intense and sharper with respect to those observed for the BM sample, as shown in **Figure 2A, 200 °C**. Variations in the band intensity and shape due to thermal cycling of the BM sample can be related to the release of internal stress and to the formation of a coarser microstructure. A decrease in intensity of the 1185 cm^{-1} band (asymmetric bending) can be related to an modification of the BH_4^- surroundings, such as a change of neighbouring atoms or distances between the ions in the lattice, as observed for the bromide substitution in $LiBH_4$.[9] This band shows a redshift of 3 cm^{-1} with respect to the BM sample after thermal cycling. Generally, it can be observed that the typical IR bands due to the presence of $KCa(BH_4)_3$ (ν_4 and *) can be clearly assigned in the LiNaKMgCa system after thermal cycling, as shown in **Figure 2A, 200 °C.**

Moreover, a strong band, marked #, similar to the one of $Mg(BH_4)_2$, is emerging together with two unidentified bands at 772 and 751 cm^{-1}. These are very sharp and could be related to the formation of a new unknown phase, which can can be connected to the broad halo observed in the PXD pattern in **Figure 1A, 200 °C**. Similar IR bands below 800 cm^{-1} have been observed in closoboranes,[61] however the observed frequencies do not correspond to those of any known closoboranes reported in the literature.

In the Raman spectra reported in **Figure 2B, 200 °C**, some bands disappears after thermal cycling, while from the broad stretching band emerges a peak at 2306 cm^{-1}.

In order to confirm the interpretation of the observed DSC traces for the LiNaKMgCa system, the thermal behaviour of the KCa system was also investigated by DSC analysis, allowing to determine the enthalpy of the polymorphic transition and melting of the $KCa(BH_4)_3$ compound. **Figure S4** reports the DSC traces observed upon two cycles of heating up to 370 °C and cooling. For the experiment, a backpressure of 50 bar of H_2 was applied to avoid the decomposition of the bimetallic compound, which was reported to occur strictly after melting.[53,62] The polymorphic transition occurs at an onset temperature of 67 °C on the second heating cycle (T_{peak}= 72 °C) and an onset temperature of 72 °C on the second cooling cycle (T_{peak}= 66 °C) with an enthalpy of 3.5±0.1 kJ/mol. The melting occurs at an onset temperature of 356 °C on the second heating cycle (T_{peak}= 363 °C) and an onset temperature of 361 °C on the second cooling cycle (T_{peak}= 359 °C), with an enthalpy of 6.3±0.1 kJ/mol.

To better understand the thermal events observed in the DSC analysis, an *in-situ* SR-PXD experiment up to 250 °C has been performed for LiNaKMgCa system and results are shown in **Figure 3,** where the intensities of diffraction peaks are compared with HP-DSC traces upon cycling in the same temperature range. PXD patterns selected at various temperatures are reported in **Figure S5**.

From the *in-situ* analysis, it can be clearly observed the polymorphic transition of $KCa(BH_4)_3$ at T_{peak}= 78 °C on heating and T_{peak}= 59 °C on cooling. Starting from T_{peak}= 100 °C (T_{peak}= 88 °C on

cooling), the PXD peak intensities of the high temperature polymorph of $KCa(BH_4)_3$ are increasing continually, while the intensity of $LiBH_4$ and KBH_4 are clearly decreasing, due to the eutectic melting of the LiNaK ternary eutectic. On the other hand, no significant change in the $NaBH_4$ peak intensity is observed, due to the small quantity that melts in the eutectic. At T_{peak}= 113 °C (T_{peak}= 108 °C on cooling), the PXD peaks of $LiBH_4$ disappear, since it is fully dissolved in the liquid phase. Up to 150 °C, also intensities of PXD peaks from KBH_4, $Mg(BH_4)_2$ and $Ca(BH_4)_2$ are decreasing. At 190 °C (T_{peak}= 184 °C on cooling) a broad melting peak ends in the DSC trace, and corresponding KBH_4 and $Mg(BH_4)_2$ melting is observed in SR-PXD patterns. Above 245 °C, the mixture is totally molten, and only broad peaks, that can be assigned to the liquid phase, are observed in the PXD patterns (see also **Figure S5**, from 250 °C and upon cooling).

$KCa(BH_4)_3$ and $NaBH_4$ recrystallize upon cooling at 234 °C (T_{peak}= 229 °C), as it can be observed combining the DSC trace and the SR-PXD patterns. Additionally, the same transformations that are observed on heating are reversible upon cooling and can be detected in the DSC trace, but crystalline phases are hardly visible in the PXD. **Figure S6** compares the RT scans before (**black, dashed dot line**) and after (**red, continuous line**) the *in-situ* thermal cycling. After the annealing treatment, only $KCa(BH_4)_3$ and $NaBH_4$ are easily recognised, while no trace of KBH_4 and $Ca(BH_4)_2$ are observed. It is worth noting that at 2θ values of 1.3°, 2.5° and 4.7°, broad diffraction peaks are observed, maybe related to an unknown disordered phase. They are similar to the ones observed in the molten mixture (**Figure S5**) and are located in similar positions of diffraction peaks of $LiBH_4$ and $Mg(BH_4)_2$.

The combined DSC and SR-PXD analyses evidence the formation of a liquid borohydride phase, in which five cations are present simultaneously. The melting temperatures observed on heating in the LiNaKMgCa system are quite in good agreement with the eutectic temperatures present in binary system, as reported in **Table 1**. In addition, it is clear that the melting sequence involves also the bimetallic borohydride, $KCa(BH_4)_3$. These results suggest limited interactions of borohydrides in the LiNaKMgCa system in the solid phase, where they result nearly immiscible. On the contrary, in

the liquid phase, they interact, promoting miscibility and forming a quinary borohydride liquid phase, here observed for the first time. This liquid phase is likely promoted by a negative enthalpy of mixing.

In principle, sufficiently high temperatures would promote an entropy-driven transition to a structure containing a random cation occupancy in only one sub-lattice. However, sometimes, this temperature is too high and the material melts before reaching it, as it was observed for the selected system in this study. The failed formation of a unique solid solution phase could be additionally justified because of a not appropriate diversity in crystal structures, coordination and cationic radii of pure borohydrides. In fact, natural tendencies to minimize polyhedral distortions, maximize space filling and adopt polyhedral linkages that preserve electroneutrality required similar crystal structures, electronegativity and cation coordination. In addition, in order to form a solid solution, ions in the system should be isovalent, such that relative cation ratios can be varied continuously with a preserved electroneutrality. In this case, the addition of both mono-valent and bi-valent light-metals borohydrides to the mixture, likely hindered the occurrence of significant solubility.

Hydrogen desorption from the quinary borohydride system

Pure light-metals borohydrides have shown to release hydrogen at relatively high temperatures and the tailoring of their thermodynamics towards a room temperature and pressure hydrogen release is of interest for real applications of these systems for hydrogen storage.[63,64] Under argon flow, alkali-borohydrides decompose after melting: $LiBH_4$ is reported to slowly start to decompose above 300 °C, even after BM,[63,65] and its main decomposition occurs above 400 °C.[63] $NaBH_4$ decomposes slowly from the solid state and the main decomposition reaction occurs, after melting, slightly above 500 °C.[51,66] Decomposition occurs after melting and above 625 °C for KBH_4 as well.[51] $Mg(BH_4)_2$ and $Ca(BH_4)_2$ are reported to decompose above 250 °C and 350 °C, respectively, under argon flow.[63] Sometimes, ball milling and nanosizing of powder can modify the hydrogen release properties of those compounds. So, to understand if hydrogen release temperatures could have been modified because of BM, DTA-MS experiments on BM pure

$Mg(BH_4)_2$, $Ca(BH_4)_2$ and the KCa system have been performed and results are reported in **Figure 4**. In all investigated samples, diborane gas was never detected in the MS analysis of decomposition gas. From the DTA-MS analysis of BM-$Mg(BH_4)_2$, the polymorphic transition of $Mg(BH_4)_2$ is observed at T_{peak}= 200 °C, together with the starting of hydrogen release from the solid state, that is recorded in a broad range of temperature. On the other hand, BM-$Ca(BH_4)_2$ shows the polymorphic transition at T_{peak}= 164 °C and the main hydrogen release occurs above 300 °C in two steps: the main one at T_{peak}= 366 °C and a second one at T_{peak}= 431 °C. In the KCa system, after the polymorphic transition and melting of $KCa(BH_4)_3$ at T_{peak}= 77 °C and T_{peak}= 362 °C, respectively, the hydrogen release starts strictly after the melting, with an intense release detected at T_{peak}= 385 °C and 479 °C.

Results of these DTA-MS measurements obtained for the quinary mixture are also reported in **Figure 4**. After DTA signals due to various phase transformations of borohydrides constitutive of the mixture, the DTA-MS peaks due to hydrogen release from the liquid phase are clearly observed. Thermal decomposition occurs in complex multistep reactions, starting from 250 °C at T_{peak}= 282, 383, 408, 430 and 454 °C, suggesting that the hydrogen release temperatures are not sensibly different from those of pure borohydrides.

In some pure borohydrides and eutectic mixtures, hydrogen release occurs from the liquid phase mainly because of kinetic reasons. When hydrogen release occurs from the liquid state, the characteristic T_{peak} of decomposition could be related on the interaction among the cations and the complex BH_4^- anion in the liquid.[40] In the case of the LiNaKMgCa system, the presence of many cations in the liquid phase seems not to influence significantly the bond strength in the complex BH_4^- anion.

After decomposition of the LiNaKMgCa system, IR and Raman spectroscopies do not detect any representative band (**Figure 2, 500 °C**). From PXD patterns (**Figure 1A, 500 °C and Figure S2C**) decomposition products, such as CaH_2, LiH, MgB_2 and the Mg high pressure cubic phase, can be

identified. KBH_4 is still present, suggesting that the quinary mixture is not fully decomposed upon heating up to 500 °C.

Conclusions

In the present study, phase stability and hydrogen release in a quinary mixture of borohydrides have been investigated for the first time. Following the concept of high entropy alloys, the investigated system is an equimolar mixture of $LiBH_4$, $NaBH_4$, KBH_4, $Mg(BH_4)_2$ and $Ca(BH_4)_2$.

The mixture was synthetized by ball milling and characterized to investigate the possible formation of new phases or solid solutions. The borohydrides result to be immiscible upon mechanical treatment up to 50 hours: pristine borohydrides are detected in the PXD after milling, together with $KCa(BH_4)_3$, whose enthalpy of formation likely overcomes entropy effect, limiting solid solubility. The bimetallic compound has been characterised and its polymorphic transition and melting enthalpies have been determined to be equal to 3.5±0.1 kJ/mol and 6.3±0.1 kJ/mol, respectively.

The thermal behaviour of the mixture has been characterized by in-situ SR-PXD and HP-DSC. The thermal analysis reveals several melting events, up to 250 °C. So, above 250 °C, a five-component liquid borohydride has been obtained for the first time, via eutectic reactions involving a bimetallic borohydride.

After thermal cycling up to 200 °C, IR spectroscopy reveals the presence of two unknown sharp bands below 800 cm^{-1} that could be related to broad peaks observed in the PXD, suggesting the formation of an unknown phase.

Dehydrogenation from the liquid phase containing five different borohydrides occurs in a complex multistep reaction. Hydrogen release temperatures are not significantly lowered with respect to those of pure borohydrides. Not all the borohydrides have been decomposed during the thermal treatment up to 500 °C.

In conclusion, this study showed the existence of ternary or higher eutectic mixtures of borohydrides, that might be further characterised to determine the exact composition and melting temperature. In addition, the occurrence of a new unknown phase has been observed, suggesting

further studies to characterized it. More fundamental thermodynamic studies and assessments of complex systems might lead to a better understanding of phase mixtures formed upon mixing different borohydrides. Studies on their hydrogen release properties might be of interest for a further tailoring of borohydride systems for solid-state energy storage.

Acknowledgement

Financial support from the European Fuel Cells and Hydrogen Joint Undertaking in the framework of BOR4STORE (Grant agreement no. 303428) is thankfully acknowledged. European Marie Curie Actions under ECOSTORE grant agreement no. 607040 is acknowledged for supporting this work. The Erasmus Traineeship Programme is acknowledged for the financial support in the exchange mobility period between the HZG and the University of Turin. We also thank the Helmholtz Energy Materials Characterization platform (HEMCP) for instrumental support.

Supporting Information Description

ESI contains Rietveld refinements of pure BM starting borohydrides, KCa system BM and after thermal cycling, and LiNaKMgCa system BM and after thermal treatments at 200 °C and 500 °C. Weight fractions and cell parameters of all phases are reported. Furthermore, HP-DSC cycling on KCa system is reported. Finally, an insight of the *in-situ* analysis containing selected PXD patterns (every 10 °C) and a comparison of RT scans before and after *in-situ* thermal cycling are presented.

References

1. Paskevicius, M.; Jepsen, L. H.; Schouwink, P.; Černý, R.; Ravnsbæk, D. B.; Filinchuk, Y.; Dornheim, M.; Besenbacher, F.; Jensen, T. R. Metal borohydrides and derivatives – synthesis, structure and properties. *Chem. Soc. Rev.* **2017**, *46*, 1565–1634.
2. Callini, E.; Atakli, Z. Ö. K.; Hauback, B. C.; Orimo, S. I.; Jensen, C.; Dornheim, M.; Grant, D.; Cho, Y. W.; Chen, P.; Hjörvarsson, B.; de Jongh, P.; Weidenthaler, C.; Baricco, M.; Paskevicius, M.; Jensen, T. R.; Bowden, M. E.; Autrey, T. S.; Züttel, A. Complex and liquid hydrides for energy storage. *Appl. Phys. A* **2016**, *122*, 353.
3. Hino, S.; Fonneløp, J. E.; Corno, M.; Zavorotynska, O.; Damin, A.; Richter, B.; Baricco, M.; Jensen, T. R.; Sørby, M. H.; Hauback, B. C. Halide substitution in magnesium borohydride. *J. Phys. Chem. C* **2012**, *116*, 12482–12488.
4. Rude, L. H.; Groppo, E.; Arnbjerg, L. M.; Ravnsbæk, D. B.; Malmkjær, R. A.; Filinchuk, Y.; Baricco, M.; Besenbacher, F.; Jensen, T. R. Iodide substitution in lithium borohydride, LiBH4–LiI. *J. Alloys Compd.* **2011**, *509*, 8299–8305.
5. Olsen, J. E.; Karen, P.; Sørby, M. H.; Hauback, B. C. Effect of chloride substitution on the order-disorder transition in NaBH4 and Na11BD4. *J. Alloys Compd.* **2014**, *587*, 374–379.
6. Grove, H.; Rude, L. H.; Jensen, T. R.; Corno, M.; Ugliengo, P.; Baricco, M.; Sørby, M. H.; Hauback, B. C. Halide substitution in Ca(BH 4) 2. *RSC Adv.* **2014**, *4*, 4736–4742.
7. Rude, L. H.; Filinchuk, Y.; Sørby, M. H.; Hauback, B. C.; Besenbacher, F.; Jensen, T. R. Anion Substitution in Ca(BH 4) 2 −CaI 2 : Synthesis, Structure and Stability of Three New Compounds. *J. Phys. Chem. C* **2011**, *115*, 7768–

7777.
8. Ravnsbæk, D. B.; Rude, L. H.; Jensen, T. R. Chloride substitution in sodium borohydride. *J. Solid State Chem.* **2011**, *184*, 1858–1866.
9. Rude, L. H.; Zavorotynska, O.; Arnbjerg, L. M.; Ravnsbæk, D. B.; Malmkjær, R. A.; Grove, H.; Hauback, B. C.; Baricco, M.; Filinchuk, Y.; Besenbacher, F.; Jensen, T. R. Bromide substitution in lithium borohydride, LiBH4–LiBr. *Int. J. Hydrogen Energy* **2011**, *36*, 15664–15672.
10. Arnbjerg, L. M.; Ravnsbæk, D. B.; Filinchuk, Y.; Vang, R. T.; Cerenius, Y.; Besenbacher, F.; Jørgensen, J.-E.; Jakobsen, H. J.; Jensen, T. R. Structure and Dynamics for LiBH4−LiCl Solid Solutions. *Chem. Mater.* **2009**, *21*, 5772–5782.
11. Zavorotynska, O.; Corno, M.; Pinatel, E. R.; Rude, L. H.; Ugliengo, P.; Jensen, T. R.; Baricco, M. Theoretical and Experimental Study of LiBH4-LiCl Solid Solution. *Crystals* **2012**, *2*, 144–158.
12. Corno, M.; Pinatel, E. R.; Ugliengo, P.; Baricco, M. A computational study on the effect of fluorine substitution in LiBH4. *J. Alloys Compd.* **2011**, *509*, S679–S683.
13. Rude, L. H.; Filsø, U.; D'Anna, V.; Spyratou, A.; Richter, B.; Hino, S.; Zavorotynska, O.; Baricco, M.; Sørby, M. H.; Hauback, B. C.; Hagemann, H.; Besenbacher, F.; Skibsted, J.; Jensen, T. R. Hydrogen–fluorine exchange in NaBH4–NaBF4. *Phys. Chem. Chem. Phys.* **2013**, *15*, 18185.
14. Pinatel, E. R.; Corno, M.; Ugliengo, P.; Baricco, M. Effects of metastability on hydrogen sorption in fluorine substituted hydrides. *J. Alloys Compd.* **2014**, *615*, S706–S710.
15. Richter, B.; Ravnsbæk, D. B.; Sharma, M.; Spyratou, A.; Hagemann, H.; Jensen, T. R. Fluoride substitution in LiBH 4 ; destabilization and decomposition. *Phys. Chem. Chem. Phys.* **2017**, *19*, 30157–30165.
16. Nielsen, T. K.; Besenbacher, F.; Jensen, T. R. Nanoconfined hydrides for energy storage. *Nanoscale* **2011**, *3*, 2086.
17. Wang, K.; Kang, X.; Ren, J.; Wang, P. Nanostructured graphite-induced destabilization of LiBH 4 for reversible hydrogen storage. *J. Alloys Compd.* **2016**, *685*, 242–247.
18. Dematteis, E. M.; Vaunois, S.; Pistidda, C.; Dornheim, M.; Baricco, M. Reactive Hydride Composite of Mg2NiH4 with Borohydrides Eutectic Mixtures. *Crystals* **2018**, *8*, 90.
19. Pottmaier, D.; Pistidda, C.; Groppo, E.; Bordiga, S.; Spoto, G.; Dornheim, M.; Baricco, M. Dehydrogenation reactions of 2NaBH4 + MgH2 system. *Int. J. Hydrogen Energy* **2011**, *36*, 7891–7896.
20. Dematteis, E. M.; Roedern, E.; Pinatel, E. R.; Corno, M.; Jensen, T. R.; Baricco, M. A thermodynamic investigation of the LiBH4–NaBH4 system. *RSC Adv.* **2016**, *6*, 60101–60108.
21. Dematteis, E. M.; Pinatel, E. R.; Corno, M.; Jensen, T. R.; Baricco, M. Phase diagrams of the LiBH4–NaBH4–KBH4 system. *Phys. Chem. Chem. Phys.* **2017**, *19*, 25071–25079.
22. Cantor, B.; Chang, I. T. H.; Knight, P.; Vincent, A. J. B. Microstructural development in equiatomic multicomponent alloys. *Mater. Sci. Eng. A* **2004**, *375–377*, 213–218.
23. Poletti, M. G.; Battezzati, L. Electronic and thermodynamic criteria for the occurrence of high entropy alloys in metallic systems. *Acta Mater.* **2014**, *75*, 297–306.
24. Yeh, J.-W.; Chen, S.-K.; Lin, S.-J.; Gan, J.-Y.; Chin, T.-S.; Shun, T.-T.; Tsau, C.-H.; Chang, S.-Y. Nanostructured High-Entropy Alloys with Multiple Principal Elements: Novel Alloy Design Concepts and Outcomes. *Adv. Eng. Mater.* **2004**, *6*, 299–303.
25. Laurent-Brocq, M.; Akhatova, A.; Perrière, L.; Chebini, S.; Sauvage, X.; Leroy, E.; Champion, Y. Insights into the phase diagram of the CrMnFeCoNi high entropy alloy. *Acta Mater.* **2015**, *88*, 355–365.
26. Senkov, O. N.; Woodward, C.; Miracle, D. B. Microstructure and Properties of Aluminum-Containing Refractory High-Entropy Alloys. *Jom* **2014**, *66*, 2030–2042.
27. Senkov, O. N.; Wilks, G. B.; Scott, J. M.; Miracle, D. B. Mechanical properties of Nb25Mo25Ta25W25 and V20Nb20Mo20Ta20W20 refractory high entropy alloys. *Intermetallics* **2011**, *19*, 698–706.
28. Li, Z.; Pradeep, K. G.; Deng, Y.; Raabe, D.; Tasan, C. C. Metastable high-entropy dual-phase alloys overcome the strength–ductility trade-off. *Nature* **2016**, *534*, 227–230.
29. Miracle, D.; Miller, J.; Senkov, O.; Woodward, C.; Uchic, M.; Tiley, J. Exploration and Development of High Entropy Alloys for Structural Applications. *Entropy* **2014**, *16*, 494–525.
30. Miracle, D. B.; Senkov, O. N. A critical review of high entropy alloys and related concepts. *Acta Mater.* **2017**, *122*, 448–511.
31. Rogal, L.; Bobrowski, P.; Körmann, F.; Divinski, S.; Stein, F.; Grabowski, B. Computationally-driven engineering of sublattice ordering in a hexagonal AlHfScTiZr high entropy alloy. *Sci. Rep.* **2017**, *7*, 2209.
32. Santodonato, L. J.; Zhang, Y.; Feygenson, M.; Parish, C. M.; Gao, M. C.; Weber, R. J. K.; Neuefeind, J. C.; Tang, Z.; Liaw, P. K. Deviation from high-entropy configurations in the atomic distributions of a multi-principal-element alloy. *Nat. Commun.* **2015**, *6*, 5964.
33. Feuerbacher, M. Dislocations and deformation microstructure in a B2-ordered Al28Co20Cr11Fe15Ni26 high-entropy alloy. *Sci. Rep.* **2016**, *6*, 29700.
34. Andersson, J.-O.; Guillermet, A. F.; Hillert, M.; Jansson, B.; Sundman, B. A compound-energy model of ordering in a phase with sites of different coordination numbers. *Acta Metall.* **1986**, *34*, 437–445.
35. Rost, C. M.; Sachet, E.; Borman, T.; Moballegh, A.; Dickey, E. C.; Hou, D.; Jones, J. L.; Curtarolo, S.; Maria, J.-P. Entropy-stabilized oxides. *Nat. Commun.* **2015**, *6*, 8485.
36. Gild, J.; Zhang, Y.; Harrington, T.; Jiang, S.; Hu, T.; Quinn, M. C.; Mellor, W. M.; Zhou, N.; Vecchio, K.; Luo, J.

High-Entropy Metal Diborides: A New Class of High-Entropy Materials and a New Type of Ultrahigh Temperature Ceramics. *Sci. Rep.* **2016**, *6*, 2–11.
37. Jiang, S.; Hu, T.; Gild, J.; Zhou, N.; Nie, J.; Qin, M.; Harrington, T.; Vecchio, K.; Luo, J. A new class of high-entropy perovskite oxides. *Scr. Mater.* **2018**, *142*, 116–120.
38. El Kharbachi, A.; Pinatel, E. R.; Nuta, I.; Baricco, M. A thermodynamic assessment of LiBH4. *Calphad* **2012**, *39*, 80–90.
39. Orimo, S. I.; Nakamori, Y.; Kitahara, G.; Miwa, K.; Ohba, N.; Towata, S.; Züttel, A. Dehydriding and rehydriding reactions of LiBH4. *J. Alloys Compd.* **2005**, *404–406*, 427–430.
40. Liu, Y.; Reed, D.; Paterakis, C.; Contreras Vasquez, L.; Baricco, M.; Book, D. Study of the decomposition of a 0.62LiBH4–0.38NaBH4 mixture. *Int. J. Hydrogen Energy* **2017**, *42*, 22480–22488.
41. Ley, M. B.; Roedern, E.; Jensen, T. R. Eutectic melting of LiBH4–KBH4. *Phys. Chem. Chem. Phys.* **2014**, *16*, 24194–24199.
42. Roedern, E.; Hansen, B. R. S.; Ley, M. B.; Jensen, T. R. Effect of Eutectic Melting, Reactive Hydride Composites, and Nanoconfinement on Decomposition and Reversibility of LiBH 4 –KBH 4. *J. Phys. Chem. C* **2015**, *119*, 25818–25825.
43. Bardají, E. G.; Zhao-Karger, Z.; Boucharat, N.; Nale, A.; van Setten, M. J.; Lohstroh, W.; Röhm, E.; Catti, M.; Fichtner, M. LiBH 4 −Mg(BH 4) 2 : A Physical Mixture of Metal Borohydrides as Hydrogen Storage Material. *J. Phys. Chem. C* **2011**, *115*, 6095–6101.
44. Liu, X.; Peaslee, D.; Sheehan, T. P.; Majzoub, E. H. Decomposition Behavior of Eutectic LiBH4–Mg(BH4)2 and Its Confinement Effects in Ordered Nanoporous Carbon. *J. Phys. Chem. C* **2014**, *118*, 27265–27271.
45. Fang, Z.-Z.; Kang, X.-D.; Wang, P.; Li, H.-W.; Orimo, S.-I. Unexpected dehydrogenation behavior of LiBH4/Mg(BH4)2 mixture associated with the in situ formation of dual-cation borohydride. *J. Alloys Compd.* **2010**, *491*, L1–L4.
46. Lee, J. Y.; Ravnsbæk, D. B.; Lee, Y. S.; Kim, Y.; Cerenius, Y.; Shim, J.; Jensen, T. R.; Hur, N. H.; Cho, Y. W. Decomposition Reactions and Reversibility of the LiBH4 -Ca(BH4)2 Composite. *J. Phys. Chem. C* **2009**, *113*, 15080–15086.
47. Lee, H. S.; Lee, Y. S.; Suh, J. Y.; Kim, M.; Yu, J. S.; Cho, Y. W. Enhanced Desorption and Absorption Properties of Eutectic LiBH4-Ca(BH4)2 Infiltrated into Mesoporous Carbon. *J. Phys. Chem. C* **2011**, *115*, 20027–20035.
48. Milanese, C.; Garroni, S.; Girella, A.; Mulas, G.; Berbenni, V.; Bruni, G.; Suriñach, S.; Baró, M. D.; Marini, A. Thermodynamic and Kinetic Investigations on Pure and Doped NaBH 4 −MgH 2 System. *J. Phys. Chem. C* **2011**, *115*, 3151–3162.
49. Jensen, S. R. H.; Jepsen, L. H.; Skibsted, J.; Jensen, T. R. Phase Diagram for the NaBH4-KBH4 System and the Stability of a Na(1– x)K(x)BH4 Solid Solution. *J. Phys. Chem. C* **2015**, *119*, 27919–27929.
50. Ley, M. B.; Roedern, E.; Thygesen, P.; Jensen, T. R. Melting Behavior and Thermolysis of NaBH4−Mg(BH4)2 and NaBH4−Ca(BH4)2 Composites. *Energies* **2015**, *8*, 2701–2713.
51. Stasinevich, D. S.; Egorenko, G. A. Thermographic Investigation of Alkali Metal and Magnesium Tetrahydroborates at pressures up to 10 atm. *Russ. J. Inorg. Chem.* **1968**, *13*, 341–343.
52. Schouwink, P.; D'Anna, V.; Ley, M. B.; Lawson Daku, L. M.; Richter, B.; Jensen, T. R.; Hagemann, H.; Černý, R. Bimetallic Borohydrides in the System M (BH 4) 2 –KBH 4 (M = Mg, Mn): On the Structural Diversity. *J. Phys. Chem. C* **2012**, *116*, 10829–10840.
53. Schouwink, P.; Ley, M. B.; Tissot, A.; Hagemann, H.; Jensen, T. R.; Smrčok, L.; Černý, R. Structure and properties of complex hydride perovskite materials. *Nat. Commun.* **2014**, *5706*, 1–10.
54. Pinatel, E. R.; Albanese, E.; Civalleri, B.; Baricco, M. Thermodynamic modelling of Mg(BH4)2. *J. Alloys Compd.* **2015**, *645*, S64–S68.
55. Borgschulte, A.; Gremaud, R.; Züttel, A.; Martelli, P.; Remhof, A.; Ramirez-Cuesta, A. J.; Refson, K.; Bardaji, E. G.; Lohstroh, W.; Fichtner, M.; Hagemann, H.; Ernst, M. Experimental evidence of librational vibrations determining the stability of calcium borohydride. *Phys. Rev. B* **2011**, *83*, 24102.
56. Mao, J.; Guo, Z.; Poh, C. K.; Ranjbar, A.; Guo, Y.; Yu, X.; Liu, H. Study on the dehydrogenation kinetics and thermodynamics of Ca(BH4)2. *J. Alloys Compd.* **2010**, *500*, 200–205.
57. Lutterotti, L.; Matthies, S.; Wenk, H. R. MAUD: a friendly Java program for material analysis using diffraction. *IUCr Newsl. CPD* **1999**, *21*, 14–15.
58. Bösenberg, U.; Pistidda, C.; Tolkiehn, M.; Busch, N.; Saldan, I.; Suarez-Alcantara, K.; Arendarska, A.; Klassen, T.; Dornheim, M. Characterization of metal hydrides by in-situ XRD. *Int. J. Hydrogen Energy* **2014**, *39*, 9899–9903.
59. Filinchuk, Y.; Richter, B.; Jensen, T. R.; Dmitriev, V.; Chernyshov, D.; Hagemann, H. Porous and Dense Magnesium Borohydride Frameworks: Synthesis, Stability, and Reversible Absorption of Guest Species. *Angew. Chemie Int. Ed.* **2011**, *50*, 11162–11166.
60. D'Anna, V.; Spyratou, A.; Sharma, M.; Hagemann, H. FT-IR spectra of inorganic borohydrides. *Spectrochim. Acta Part A Mol. Biomol. Spectrosc.* **2014**, *128*, 902–906.
61. Muetterties, E. L.; Merrifield, R. E.; Miller, H. C.; Knoth, W. H.; Downing, J. R. Chemistry of Boranes. III. 1 The Infrared and Raman Spectra of B 12 H 12 - and Related Anions. *J. Am. Chem. Soc.* **1962**, *84*, 2506–2508.
62. Schouwink, P.; Ramel, A.; Giannini, E.; Černý, R. Flux-assisted single crystal growth and heteroepitaxy of perovskite-type mixed-metal borohydrides. *CrystEngComm* **2015**, *17*, 2682–2689.

63. Paskevicius, M.; Ley, M. B.; Sheppard, D. A.; Jensen, T. R.; Buckley, C. E. Eutectic melting in metal borohydrides. *Phys. Chem. Chem. Phys.* **2013**, *15*, 19774.
64. Rude, L. H.; Nielsen, T. K.; Ravnsbæk, D. B.; Bösenberg, U.; Ley, M. B.; Richter, B.; Arnbjerg, L. M.; Dornheim, M.; Filinchuk, Y.; Besenbacher, F.; Jensen, T. R. Tailoring properties of borohydrides for hydrogen storage: A review. *Phys. status solidi* **2011**, *208*, 1754–1773.
65. Lang, J.; Gerhauser, A.; Filinchuk, Y.; Klassen, T.; Huot, J. Differential Scanning Calorimetry (DSC) and Synchrotron X-ray Diffraction Study of Unmilled and Milled LiBH4: A Partial Release of Hydrogen at Moderate Temperatures. *Crystals* **2011**, *2*, 1–21.
66. Urgnani, J.; Torres, F. J.; Palumbo, M.; Baricco, M. Hydrogen release from solid state NaBH4. *Int. J. Hydrogen Energy* **2008**, *33*, 3111–3115.

Figure

Dematteis et al. – Figure 1

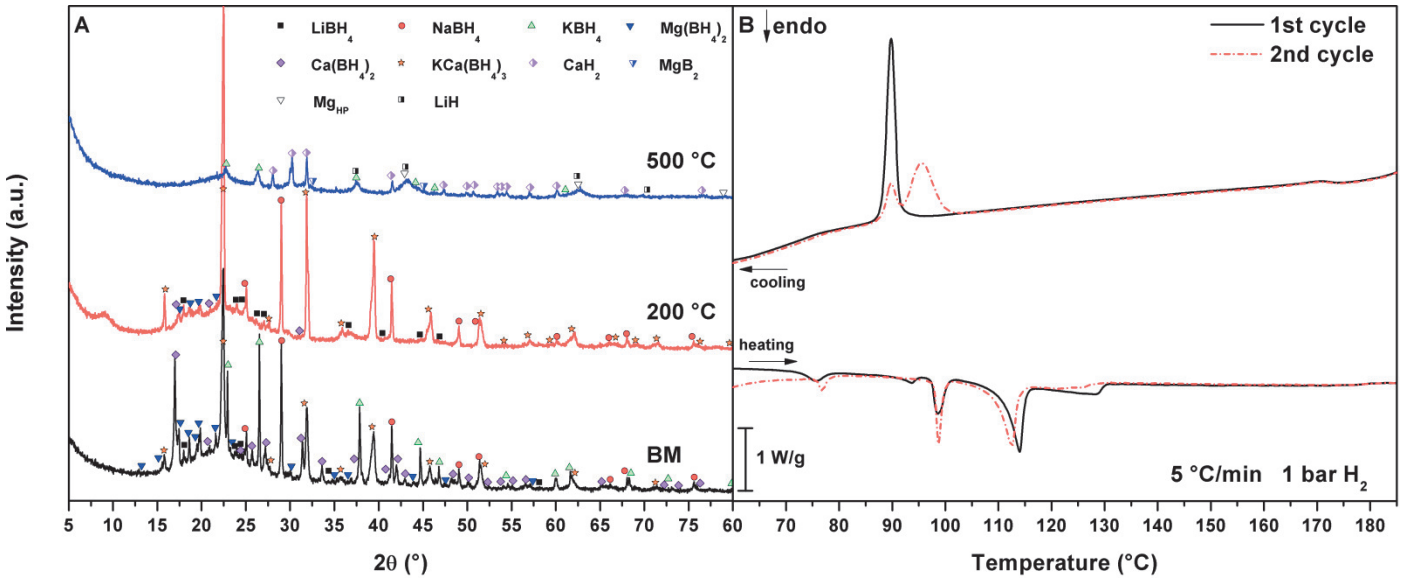

Figure 1 – LiNaKMgCa system: A) PXD pattern of samples ball milled (BM) and annealed in DSC up to 200 °C and 500 °C, B) HP-DSC trace, 2 cycle of heating and cooling at 5 °C/min and 1 bar of H_2.

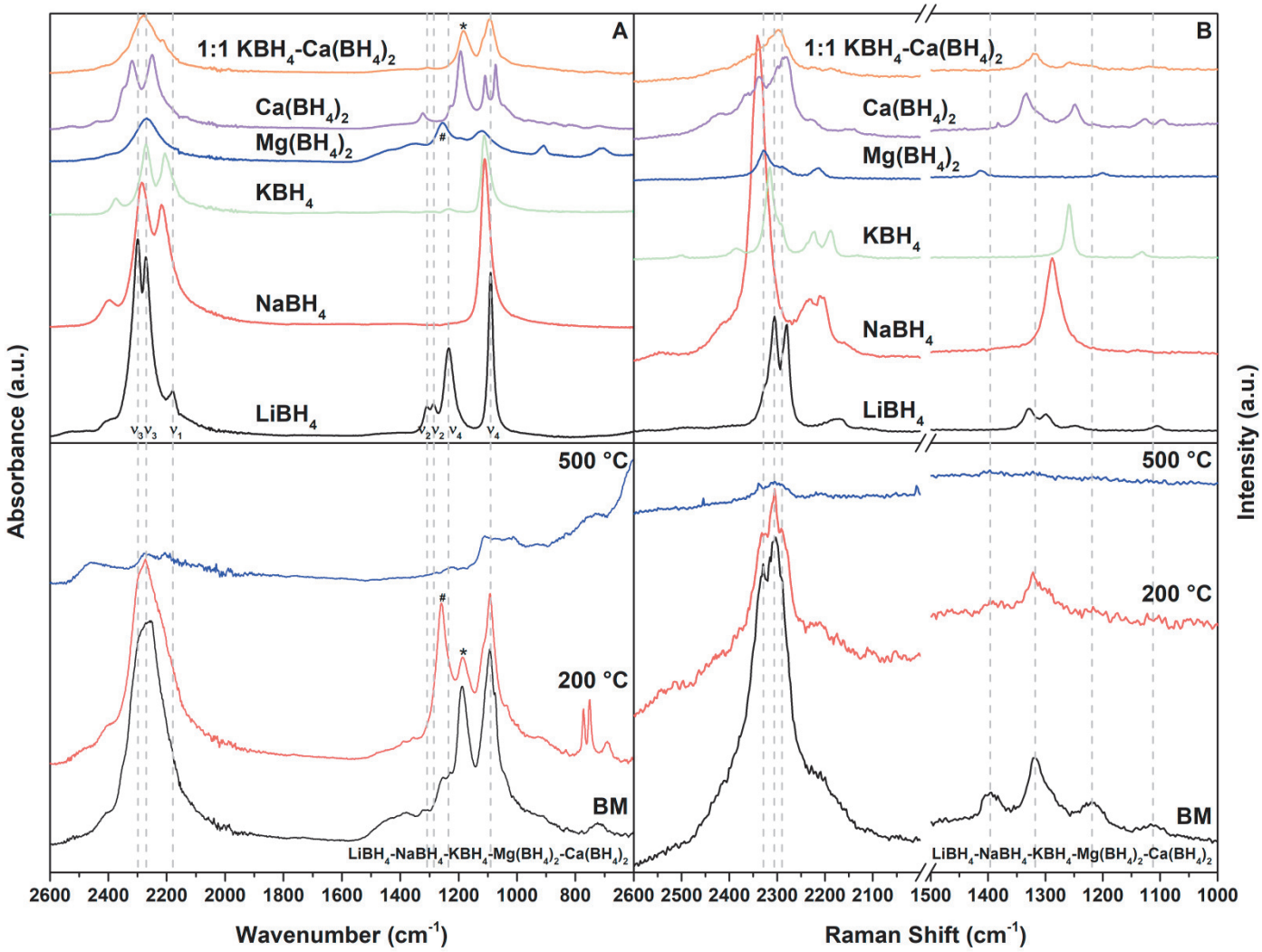

Figure 2 – ATR-IR (A) and Raman (B) spectra of ball milling pure borohydrides and KCa system (top) and LiNaKMgCa system after ball milling (BM) and after annealing at 200 °C and 500 °C (bottom).

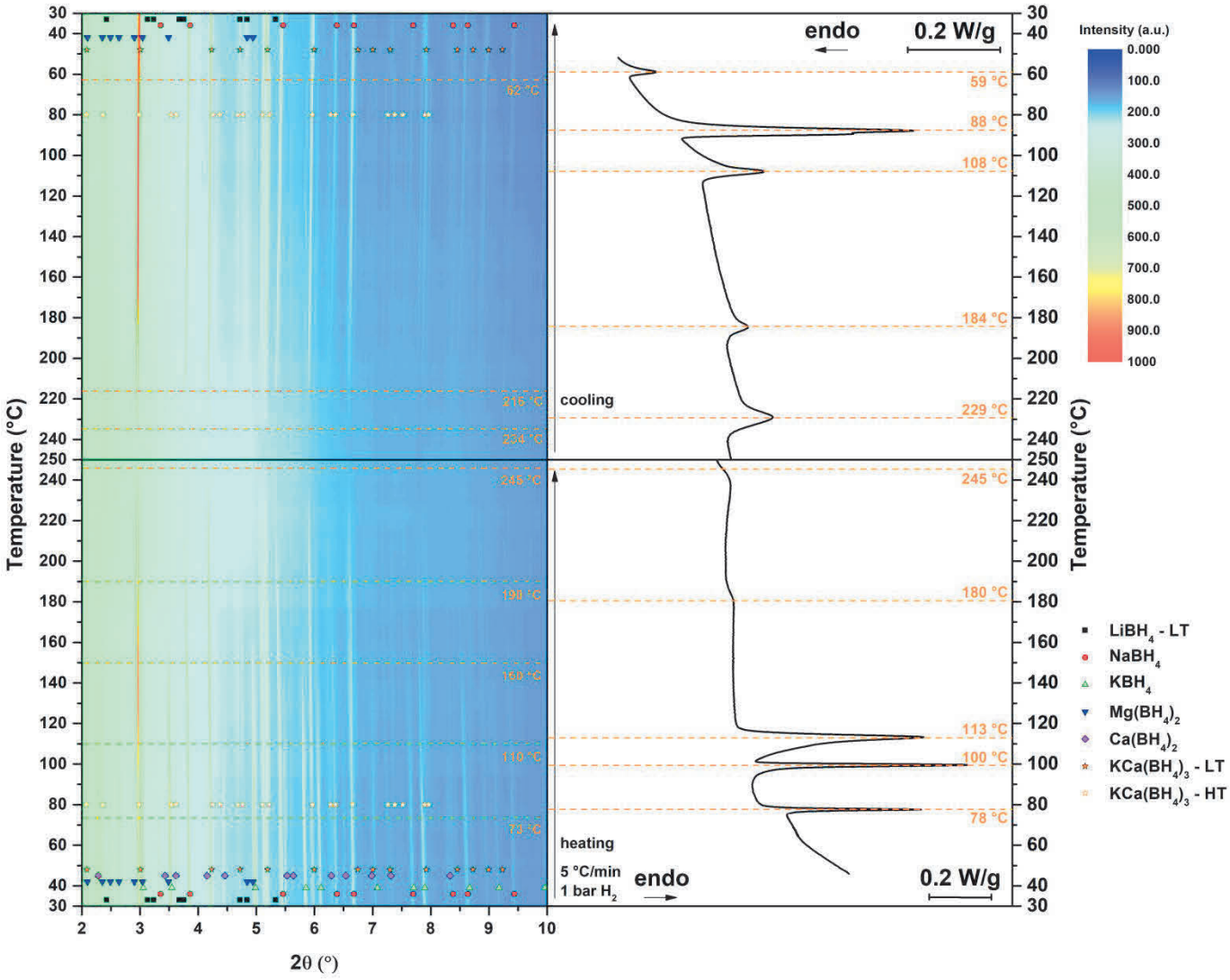

Figure 3 – LiNaKMgCa system: *in-situ* SR-PXD (left) up to 250 °C on heating and cooling at 5 °C/min and 1 bar of H_2 compared with HP-DSC trace (right) in the same condition.

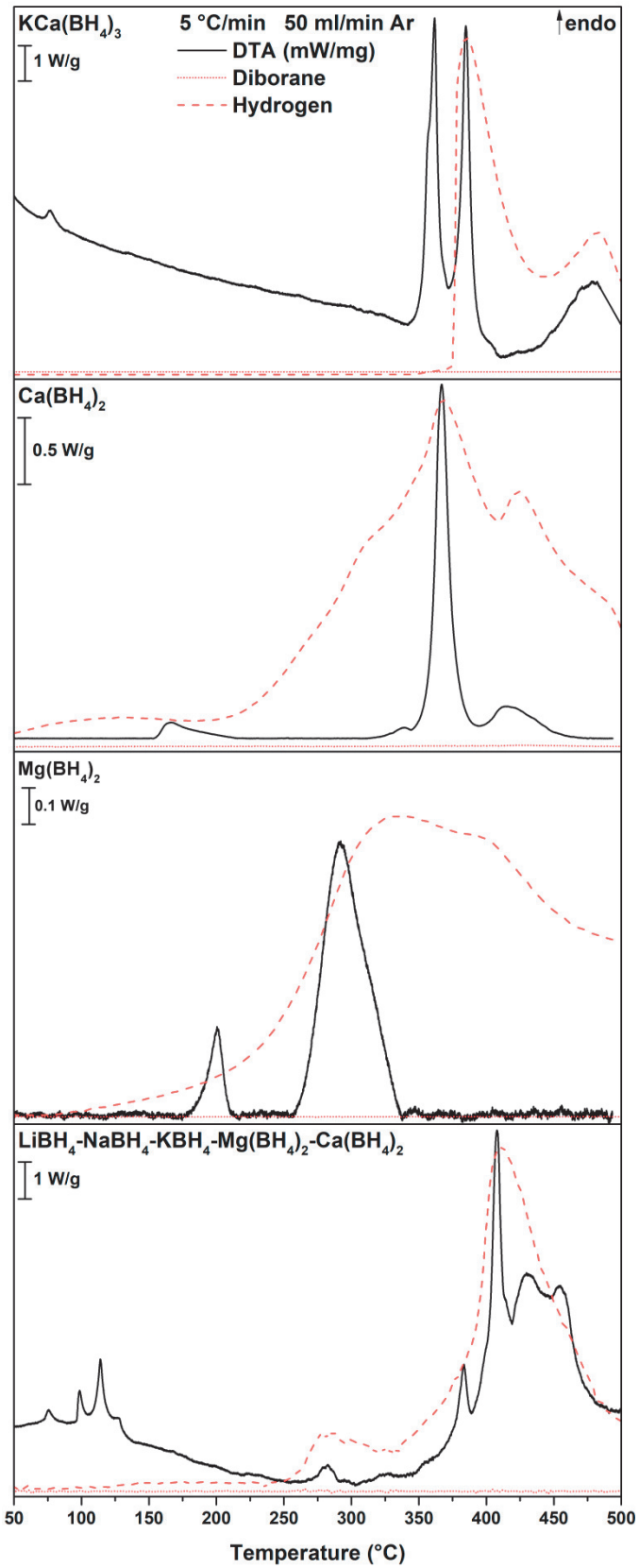

Figure 4 – DTA trace and MS of hydrogen and diborane up to 500°C, 5 °C/min, 50 mL/min Argon flow of LiNaKMgCa system compared with pure BM $Mg(BH_4)_2$, $Ca(BH_4)_2$ and the KCa system.